Journal of Environmental Management 366 (2024) 121595

Contents lists available at ScienceDirect

Journal of Environmental Management

journal homepage: www.elsevier.com/locate/jenvman

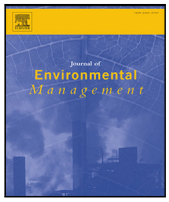

Research article

Assessing the cooling potential of climate change adaptation measures in rural areas

Beate Zimmermann [a,*], Sarah Kruber [a], Claas Nendel [b,c], Henry Munack [d], Christian Hildmann [a]

[a] Research Institute for Post-Mining Landscapes, Brauhausweg 2, Finsterwalde, 03238, Brandenburg, Germany
[b] Leibniz Centre for Agricultural Landscape Research (ZALF), Eberswalder Straße 84, Müncheberg, 15374, Brandenburg, Germany
[c] Institute of Biochemistry and Biology, Am Mühlenberg 3, Potsdam, 14476, Brandenburg, Germany
[d] Faculty of Science, Medicine and Health, School of Earth, Atmospheric and Life Sciences, and ARC Centre of Excellence for Australian Biodiversity and Heritage, Northfields Ave Wollongong, Wollongong, 2522, NSW, Australia

ARTICLE INFO

Dataset link: https://earthexplorer.usgs.gov/, https://land.copernicus.eu/en, https://www.dwd.de/EN/

Keywords:
Climate change adaptation
Land surface temperature
Water retention
Evapotranspiration
Cooling effect
Measure evaluation

ABSTRACT

Atmospheric heat has become a major public concern in a rapidly warming world. Evapotranspiration, however, provides effective land surface cooling during the vegetation period. Adversely, modern cultural landscapes – due to both water and potential evapotranspiration pathways lacking – are increasingly incapable of offering this important benefit.

We hypothesised that concerted measures for a revived landscape water retention can fuel plant transpiration, especially during dry periods, and thus contribute to climate change adaptation by stabilising the regional climate. Seeking nature-based ways to an improved landscape water retention, we used the land surface temperature (LST) as a proxy for landscape mesoclimate. For our drought-prone rural study area, we identified potential candidate environmental predictors for which we established statistical relationships to LST. We then, from a set of potential climate change adaptation measures, mapped selected items to potential locations of implementation. Building on that, we evaluated a certain measures' probable cooling effect using (i) the fitted model and (ii) the expected expression of predictors before and after a hypothetical measure implementation.

In the modelling, we took into account the spatial and temporal autocorrelation of the LST data and thus achieved realistic parameter estimates. Using the candidate predictor set and the model, we were able to establish a ranking of the effectiveness of climate adaptation measures. However, due to the spatial variability of the predictors, the modelled LST is site-specific. This results in a spatial differentiation of a measure's benefit. Furthermore, seasonal variations occur, such as those caused by plant growth. On average, the afforestation of arable land or urban brownfields, and the rewetting of former wet meadows have the largest cooling capacities of up to 3.5 K. We conclude that heat countermeasures based on fostering both evapotranspiration and landscape water retention, even in rural regions, offer promising adaptation ways to atmospheric warming.

1. Introduction

In 2022, after a continuous 2014–2020 series of warmest years on record (Copernicus, 2022), Europe experienced its hottest summer ever recorded, with temperatures at 2.3 K above the pre-industrial benchmark level (World Meteorological Organization (WMO), 2023). The line-up of adverse impacts of rising temperatures, involving heat and drought extremes, can hardly be overestimated. For Europe, the IPCC (Bednar-Friedl et al., 2023), in light of the global warming peril, has identified four key risks (kr) – heat-related health issues (kr1), heat and drought stress on crops (kr2), water scarcity (kr3), and hydrological extremes (kr4) – which are consistently related to heat and water.

The term "heat" in this context commonly refers to sensible heat of the surrounding air that exceeds a comfort temperature threshold, and that may even become critical for physiological processes of organisms, including humans. Air temperature is a result of (i) the turnover of incoming radiation at the surface into sensible heat of the sunlit material, while a remaining fraction is reflected into the atmosphere and (ii) atmospheric transport processes that exchange air volumes of different heat content dynamically across a large range of temporal and spatial scales. In soils, a considerable fraction of the substrate is liquid water, which, when heated, may turn into vapour and evaporate from the soils' surface. The change of the state of aggregation requires energy,

* Corresponding author.
E-mail addresses: b.zimmermann@fib-ev.de (B. Zimmermann), s.kruber@fib-ev.de (S. Kruber), claas.nendel@zalf.de (C. Nendel), hmunack@uow.edu.au (H. Munack), c.hildmann@fib-ev.de (C. Hildmann).

https://doi.org/10.1016/j.jenvman.2024.121595
Received 15 December 2023; Received in revised form 30 April 2024; Accepted 23 June 2024
Available online 10 July 2024

and this consumption results in a turnover of sensible into latent heat and an immediate temperature decrease of the surrounding media, a local net cooling effect. The same principle applies when liquid water turns into vapour in the stomata of plants and then transpires from the plants surface. The cooling effect of transpiration protects plants against extreme heat, as critically high temperatures may cause damage to plant tissue.

A s a consequence of the complex interaction of many factors, transpiration is highly dynamic in both space and time. The vegetation's influence on the surrounding microclimate increases with both the number of plants and their transpiring surface. This causes any vegetation, yet to different degree, to develop their own specific microclimate. Depending on the vegetation extent, the combined evaporation from the soil and transpiration from the vegetation, commonly referred to as *evapotranspiration*, may even influence meteorological variables at the landscape scale, referred to as the *mesoclimate*. Landscape cooling by evaporation affects atmospheric moisture dynamics and dampens land-ocean temperature contrasts, maintaining the regional hydrologic cycle (Makarieva et al., 2022). Transpired water can be condensed again with a temporal delay and spatial shift (Makarieva et al., 2023). Because long-term temperature contrasts during the warm season in the Northern Hemisphere are close to the threshold where condensation-induced moisture transport ceases, a few degrees of additional land warming can disrupt condensation-induced moisture transport. Especially during heat waves, surface cooling provided by transpiring vegetation can be critical to avoid a tipping point where the climate turns into arid conditions (Makarieva et al., 2022).

While microclimatic effects can only be measured with proximal sensing equipment, mesoclimatic effects can potentially be investigated using remote sensing methods. Three landscape properties are relevant for this: the land surface albedo (i) describes the degree to which incoming radiation is reflected into the atmosphere. Surface roughness (ii) is defined as the deviations in the direction of the normal vector of a real surface from its ideal form, usually an ideally flat surface. Land surface temperature (iii), or LST, represents the transferred energy at the phase interface of the boundary layer and, thus, provides insights into landscape energy turnover. It integrates both albedo and land surface roughness plus the meteorological variables, and is therefore considered a proxy for the landscape's mesoclimate and, within limits, also to the microclimate within vegetation stands (Hesslerová et al., 2018; Ghafarian et al., 2024). It has hence been identified as a quantitative indicator of ecosystem and landscape functioning (Hesslerová et al., 2013). Albedo and land surface roughness are variable, but follow fairly strict patterns in space and time, while LST is often highly dynamic, responding to many influencing factors. In this study, we focus on LST when investigating how the cooling service of vegetation in rural landscapes can help taking the edge of adverse landscape overheating effects.

Using satellite thermal imagery, the LST can be quantified in a high spatial and temporal resolution (e.g. Procházka et al., 2019; Hesslerová et al., 2018). Since the LST represents transferred energy at the boundary layer, it is not directly comparable with the air temperatures measured at weather stations. To date, remotely sensed LST data have been used to map urban heat islands (e.g. Alavipanah et al., 2015; Mehmood et al., 2023), but less so with regard to rural regions (Ghafarian et al., 2024). In this context, research as so far focused on disentangling the relationship between LST and environmental factors (Alavipanah et al., 2015; Bertoldi et al., 2010; Das et al., 2020; Seeberg et al., 2022; Wickham et al., 2012), for instance to locate warming and cooling spots in cities (Seeberg et al., 2022). As a result, climate adaptation strategies could be assessed, e.g. based on LST differences between built-up and green spaces (Selim et al., 2023).

Climate adaptation measures resemble each other around the globe. However, due to regionally varying global warming impacts, adaptation measures must be bespoke regional responses to a global problem. Yet many regions have in common that, prior to the advent of industrial land-use practices, water was a ubiquitous climate buffer agent. In many eastern German watersheds, land use became intensive and radical with increasing industrialisation (Baessler and Klotz, 2006). Among other interventions, lowland drainage by means of subsurface and ditch drainage was strongly advanced from the 1960s onward, as a response to a longer period of high rainfall during spring time (Ionita et al., 2020). Landscape drainage, however, leads to accelerated loss of rainwater, rendering the landscape generally drier. Lacking water anyway, and further pressured by advancing climate change, the vegetation in these areas has become increasingly drought-stressed, which has been witnessed especially in the years 2018 and following. Any attempt to re-increase vegetation growth and transpiration-mediated cooling at landscape scale (Sušnik et al., 2022; Hildmann et al., 2022) must therefore address the way pluvial water is handled. Using the landscape itself as an interim water storage is the new goal, reversing the large-scale drainage of the past decades.

A range of measures addressing different spatial scales can be taken to achieve this (Hildmann et al., 2022), starting with the establishment of green roofs in cities, and ending at large-scale measures in rural areas, such as soil organic matter enrichment to increase the water infiltration into soils, or the re-wetting of degraded wetlands.

The considerable space–time variability of evapotranspiration suggests that nature-based climate adaptation measures must differ in terms of their cooling potential. In addition, the effect of an individual measure varies from place to place and from time to time, for example due to the seasonality of vegetation cover. For decision-makers to use limited resources efficiently for climate adaptation, knowledge of the effectiveness of the measures is crucial. However, the necessary quantification of the effects on the basis of available environmental data is sparse. To help fill this knowledge gap, we have addressed the following research questions:

1. How do environmental variables influence land surface temperature in a drought-prone rural study area?
2. Based on the relationships identified, what are the prerequisites for climate adaptation measures to be effective?
3. How can the findings be used to support decision-making on climate adaptation?

2. Materials and methods

2.1. Study area

Our study area covers the Elbe-Elster-County (EEC) in southern Brandenburg, Eastern Germany. The EEC inhabits 100,902 people (Amt für Statistik Berlin-Brandenburg, 2023) on an area of 1899 km^2 of which 51% are agricultural land and 36% are forests, respectively (Amt für Statistik Berlin-Brandenburg, 2022). Settlements and traffic areas account for 10% of the total area. Cereal farming dominates the agricultural areas, while about one fourth of the agricultural land is grassland. The forested areas are dominated by pine plantations. The low population density by German standards, the high proportion of agricultural land and forest, and the absence of major cities account for the rural character of the area (Wolff et al., 2021).

Climatically, the EEC is located in the temperate climate zone. The mean annual air temperature is 9.1 °C and annual precipitation amounts to 556.9 mm (period 1971–2000, Pfeifer et al., 2021). A 1951–1980 versus 1986–2015 comparison reveals an increase of the annual mean temperature by 0.9 °C (Pfeifer et al., 2021) while the inner-annual distribution of precipitation has shifted towards lower spring and higher winter yields (1961–1990 and the 1991–2020 compared) (Zimmermann and Hildmann, 2021). Already today, the aridity index (AI) pushes the EEC into the dry sub-humid range (county-wide

Table 1
Candidate climate change adaptation measures.

Category	Measure	Description
Agriculture	Agroforestry	Combined cultivation of arable crops and perennial woody plants
Agriculture	Deep-rooting crops	Cultivation of deep-rooted arable crops
Agriculture	Landscape structure elements	Planting of woody plants on agricultural land along ditches and trails
Agriculture	Organic fertilisation	Continuous application of organic matter to arable land
Agriculture	Permanent grassland	Conversion of arable land into permanent grassland
Agriculture	Afforestation	Afforestation of marginal arable land with broad-leaved trees
Forestry	Reforestation	Reforestation of degraded forest patches
Forestry	Forest conversion	Conversion of pure conifer stands into mixed or deciduous stands
Nature conservation	Wet meadows	Rewetting of former wet meadows
Settlements	Afforestation	Afforestation of (un)sealed urban brownfields, if necessary after unsealing
Settlements	Partial unsealing	Unsealing and laying of grass pavers
Settlements	Tree groups	Planting or compaction of groups of trees
Settlements	Tree rows	Planting rows of trees
Settlements	Unsealing	Unsealing and subsequent greening of sealed urban brownfields
Water management	Ditch water management	Adapted control of farm dam heights in melioration ditches
Water management	Supporting sills	New construction of supporting sills in melioration ditches

mean of the annual AI average: 0.64, derived from the Global ET_0 and Aridity Index Database v3 in Zomer et al., 2022).

Particularly in recent years, the region has experienced some severe soil moisture droughts during the growing season. This is consistent with Samaniego et al. (2018)'s projection that the continental climate zone – where the EEC is located in – will experience negative changes in available soil water content under ongoing climate change in all seasons except winter. The observed consequences are crop yield losses, forest damage, and wetland degradation.

The soils in the region are predominantly sandy. Their low available water holding capacity, in many areas below 140 mm in the first metre of the soil profile, exacerbate the plant water deficiency during drought periods. Peat and degraded peat soils occur in fens that are often drained for agricultural use. In general, the region's very low natural drainage density is more than doubled by artificial ditches.

2.2. Measures for climate change adaptation

In our extensive rural study area, scalable, nature-based climate adaptation measures are particularly appropriate. Consequentially, we focus on measures that involve evapotranspiration of woody plants. Since the EEC increasingly suffers from water deficiency during the growing season (Section 2.1), the desired effect of evaporative cooling requires adequate water retention in the landscape. With respect to the latter, we consider 16 climate adaptation measures (Table 1), which are described in detail in Hildmann et al. (2022). However, we do neglect micro-scale measures, such as roof greening, because they do not match (i) the major challenges of a sparsely populated rural area and (ii) the resolution of the satellite imagery that we used to assess each measures' effect. (Section 2.3.1).

In order to assign the selected measures (Table 1) to candidate implementation locations, we developed specific GIS algorithms (Appendix A). A small-scale land cover land use map of our study area with a total of almost 60,000 features served as the map basis (Appendix A).

2.3. Measure evaluation

We evaluated the potential impact of the 16 candidate measures by quantifying their influence on LST. Due to a lack of reference locations in our study area, we opted against doing a comparative study, but derived environmental predictors, that are known or thought to influence LST, from available geospatial data. We then fitted a statistical relationship between these predictors and LST. We next predicted the LST for predictor values, that can be expected before and after implementation of a climate change adaptation measure. In the following we describe the data and the model used for this purpose. Fig. 1 outlines our general study workflow.

2.3.1. Data on land surface temperature

We derived the target variable *LST* from 39 atmospherically corrected Landsat 8 (Collection 2 Level 2) satellite scenes. All 39 scenes are main vegetation period (i.e., May–Sep) recordings of the years 2013 to 2020 for our study area, respectively. Pre-processing of the scenes included removal of cloud shadows (Appendix B). As the absolute values of *LST* fluctuate due to weather conditions, they were converted into relative values. The *min–max feature scaling* was used as the scaling method.

2.3.2. Predictor selection

We chose various environmental candidate predictor variables encompassing land cover, land use, landscape structure, soil, topography, and climate (Table 2).

As the basis for land cover classification, we used the biotope and land-use mapping of the federal state of Brandenburg (Landesamt für Umwelt Brandenburg, 2009). Because the reference year for the map was 2009, we made several updates, e.g. to include newly built solar parks (Appendix A). Areas with land-use / land-cover (LULC) change between 2013 and 2020 were excluded. The updated map served as the basis for both the localisation of the measures (Appendix A) and

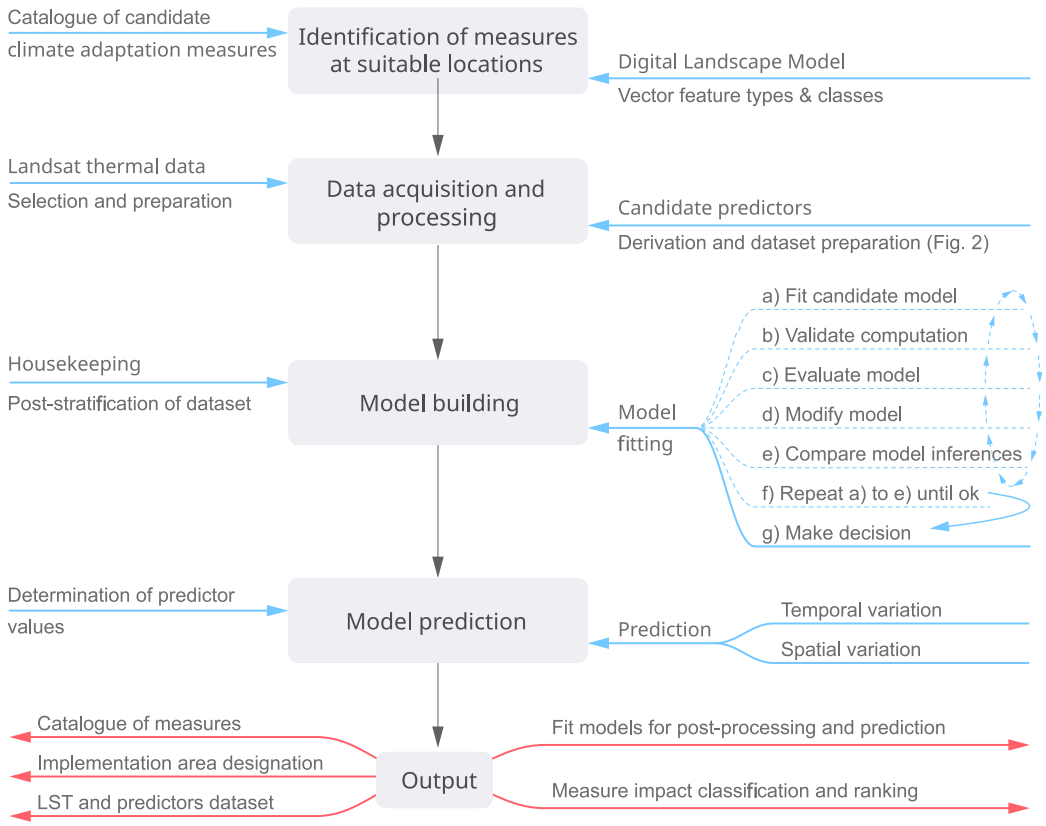

Fig. 1. Workflow.

Table 2
Candidate modelling predictors.

Predictor	Abbreviation	Type[a]	Time reference (year)	Range (unit)/No. of levels
Potential evapotranspiration	ET	Num.	Scene[b]	1 – 7.9 mm/d
Climatic water balance	CWB	Num.	Scene[c]	−140 – 51 mm/m
Land-use/land-cover class	LULC	Cat.	Static (2020)/annual[d]	13
Tree cover density	TCD	Num.	Static (2018)	0 – 1
Imperviousness density	IMD	Num.	Static (2018)	0 – 1
Core area index	CAI	Num.	Static (2020)	0.21 – 0.98
Related circumscribing circle	CIRCLE	Num.	Static (2020)	0.27 – 0.99
Available water-holding capacity	AWC	Ord.	Static (2021)	9
Terrain elevation	ELEV	Num.	Static (2004)	76 – 201 m a.s.l.

[a] Num. = numerical, Cat. = categorical, Ord. = ordinal.
[b] Daily ET on day of satellite overpass.
[c] Monthly total before the day of satellite overpass.
[d] Crop type from annual agricultural census data.

the derivation of predictors related to LULC and landscape structure. Based on predefined rules, we binned the original biotope classes into five LULC classes (Table 3). We only used classes relevant for predicting the efficacy of the climate adaptation measures. As some measures on arable land are associated with specific crop rotations, we further subdivided arable lands according to crop type (Table 3). Forests were divided into coniferous, broad-leaved and mixed forests.

Since the thermal signature of grasslands is most likely codependent on groundwater influence: during drought periods, grassland without groundwater influence tends to dry out more quickly and accordingly heats up more strongly, we opted for two matching grassland classes. However, the available EEC information resolution about groundwater is not suitable for depicting such small-scale patterns. Therefore, we chose a remotely sensed moisture index (Normalised Difference Moisture Index, NDMI) that indicates the presence or absence of a groundwater influence on plant water supply (Appendix B). By means of a histogram analysis of the NDMI composite (Appendix B), we could distinguish between "fresh" grassland areas influenced by groundwater and those that are remote from groundwater ("dry" grassland, Table 3). This enabled us to evaluate the measures "ditch water management" and "supporting sills" (Table 1).

Prior to modelling, the LULC classes *arable land*, *forest* and *grassland* were replaced with their subclasses, resulting in the predictor $LULC$ having a total of 13 levels (Table 3). In total, we included nine predictors in the analysis, which have different time references as well as different data formats (Table 2). The variables $ELEV$, ET and CWB were standardised to a mean of 0 and a standard deviation of 1 before entering them into the model.

Landscape structure metrics (LSM) were included because it is known that landscape structure influences LST (e.g. Song et al., 2014; Das et al., 2020; Kim et al., 2016). Effects such as urban heat islands (e.g. Kim et al., 2016) or the forest interior climate can thus be mapped. From the large number of available LSMs, we only considered scale-independent metrics at the patch level. We limited the remaining selection to the core area index (CAI) and the related circumscribing circle ($CIRCLE$) because of their assumed importance for LST: CAI

Table 3
LULC classes and corresponding CORINE (CLC) codes (©European Union, Copernicus Land Monitoring Service, European Environment Agency).

LULC class	Subclass	Coding	CLC code[a]
Settlements		1	1.1 to 1.4
Arable land			2.1[b]
	Alfalfa	2	
	Legumes[c]	3	
	Maize[d]	4	
	Sunflower	5	
	Winter cereals[e]	6	
	Winter oil-seed rape	7	
Grassland			2.3
	Fresh grassland[f]	8	
	Dry grassland[g]	9	
Forest	Broad-leaved forest	10	3.1.1
	Coniferous forest	11	3.1.2
	Mixed forest	12	3.1.3
Fens		13	4.1

[a] The classes 2.2, 3.2, 3.3, 4.2 and 5 are not used. Class 2.4 is either embedded in class arable land or does not exist in our study area.
[b] Except 2.1.3.
[c] Peas and lupines.
[d] Silage maize and grain maize.
[e] Spelt, winter barley, winter rye, winter triticale, winter wheat.
[f] Based on NDMI (Section 2.3.2), with assumed groundwater influence.
[g] Based on NDMI (Section 2.3.2), without assumed groundwater influence.

is used to describe effects such as heat islands, while $CIRCLE$ can be used to distinguish between linear (e.g. hedges) and clumped landscape elements. Both CAI and $CIRCLE$ are configuration metrics, which have been found to exert a stronger influence on LST than composition metrics (Du et al., 2016).

A summary of our workflow to derive the predictors from the geospatial data is provided in Fig. 2. All predictors were converted to raster data format with a resolution of 30 m (resolution of the LST data; Fig. 2). Pixels whose land-use class is not unique within a 90 m grid cell (approx. the original resolution of the Landsat Thermal Infra-Red Sensor (TIRS)) were classified as mixed pixels and excluded from the subsequent statistical analysis. In addition to the geospatial predictors, we included the pixel id (ID) and the scene number ($SCENE$) as group-level predictors in the modelling (Section 2.3.4)

2.3.3. Generation of subsets of data

The original dataset contains nearly 30 million observations: an unnecessarily large number for further analysis. In addition, the LST values are auto-correlated: a variogram analysis of the scaled LST averaged over the 39 scenes revealed a very strong and long-range spatial correlation (nugget-to-sill ratio of 0, effective range about 25 km). In order to avoid a correlation of the estimation errors and to reduce the amount of data, we applied a post-stratification routine (Appendix C).

Considering the above, we created a data subset of only 50 k observations for further analysis. We repeated subsampling three times to test the influence of the subset selection on model results. Lastly, we created a validation data subset in the same way, which does not include the three calibration data subsets.

2.3.4. Statistical modelling

Each of the 39 Landsat LST scenes was considered individually in modelling. This approach has the following advantages – (i) it avoids early data aggregation and, thus, potentially valuable information is kept, (ii) the annually varying crop type (Section 2.3.2) can be included as a time-varying modelling predictor. The latter prevents the creation of arbitrary predictor variables such as the proportion of deep-rooted plants in crop rotation. The two climatic variables (potential evapotranspiration and climatic water balance, Table 2) can also be included in the model in this way.

Given this data structure, we are dealing with a repeated measures design with censoring, since not all pixels in each scene have an LST value due to clouds. In general, the dataset is highly unbalanced because the ranges or levels of the predictors are not evenly distributed. For example the number of coniferous forest pixels is 400 times that of pixels representing fens.

Consequentially, we opted for a mixed-modelling approach, which is suitable for analysing unbalanced and incomplete data (e.g. Hesselmann, 2018). More precisely, we chose a Bayesian approach to mixed modelling due to its flexibility and intuitive interpretation of results.

We fitted nearly 100 models using iterative model building (Fig. 1, Gelman et al., 2020). Those models were run using eight chains, each with 2000 iterations, of which 1000 were used as warm-up. Most earlier candidate models had convergence problems ($\hat{R} > 2$, divergent transitions). Model modifications included the choice of response distribution and the inclusion of interaction terms.

The model used for post-processing and prediction was chosen by posterior predictive checking and model comparison among valid candidate models (Appendix D):

$$LST_{ijk} \sim T\left(\mu_{ijk}, \sigma, \nu\right) \tag{1}$$

where,

$$\begin{aligned}\mu_{ijk} &= \beta_{0,LULC[i]} + \alpha_{ID_j,LULC[i]} + \alpha_{SCENE_k,LULC[i]} + \beta_1 TCD_i + \beta_2 IMD_i \\ &+ \beta_3 ELEV_i + \beta_4 ETo_i + \beta_5 CWB_i + \beta_6 CAI_i + \beta_7 CIRCLE_i \\ &+ \beta_8(CAI_i \times LULC_i) + \beta_9(CWB_i \times LULC_i) + b \sum_{i=1}^{AWC_n} \zeta_i,\end{aligned}$$

$$\text{for } ID \text{ j} = 1, \ldots, \text{J and for } SCENE \text{ k} = 1, \ldots, \text{K}, \tag{2}$$

with,

$$\zeta_i \in [0, 1] \tag{3}$$

Eq. (1) states that the ith value of LST follows a Student distribution with mean μ, scale σ and shape ν. The subscripts j and k refer to the two grouping variables in the model (see below). We chose a Student distribution because of outliers in the residual distribution when using a Gaussian distribution.

The model has 13 population-level intercepts β_0, one for each level of $LULC$ (Eq. (2)). We chose this index-variable approach (McElreath, 2020) because it avoids dummy coding of the categorical variable $LULC$. Instead, each of the 13 levels of this categorical variable is given its own intercept.

The population-level intercepts are allowed to vary both by pixel id (ID) and by scene ($SCENE$). Hence, ID and $SCENE$ are the grouping ("random") variables, accounted for in the model by the terms $\alpha_{ID_k,LULC[i]}$ and $\alpha_{SCENE_j,LULC[i]}$. They take into account the repeated measures design and the fact that each scene is subject to certain boundary conditions (e.g. weather, season) that are not fully reflected by our population-level ("fixed") predictors. The grouping variables were considered as crossed as each pixel occurs in every scene (except missing values due to clouds).

We hypothesised that the influence of CAI on LST would vary by LULC class. For example, one might expect large settlements to be hotter than small settlements, whereas large forests should be cooler than small forest patches. Regarding possible effects of drought periods on the LST, we assumed that the effect of CWB on LST may also depend on land cover or land use, e.g., due to the different rooting depths of arable crops and forest trees. Consequently, an interaction term with $LULC$ is included for both CAI and CWB.

The predictor AWC is ordinal with nine levels (Table 2). To parametrise its regression coefficient, we used a technique called monotonic effects (Bürkner and Charpentier, 2020). The parametrisation is done in terms of a scale parameter b which represents the direction and size of the effect of AWC on LST like a "normal" regression coefficient. The second parameter, ζ, is a simplex (Eq. (3)). It describes

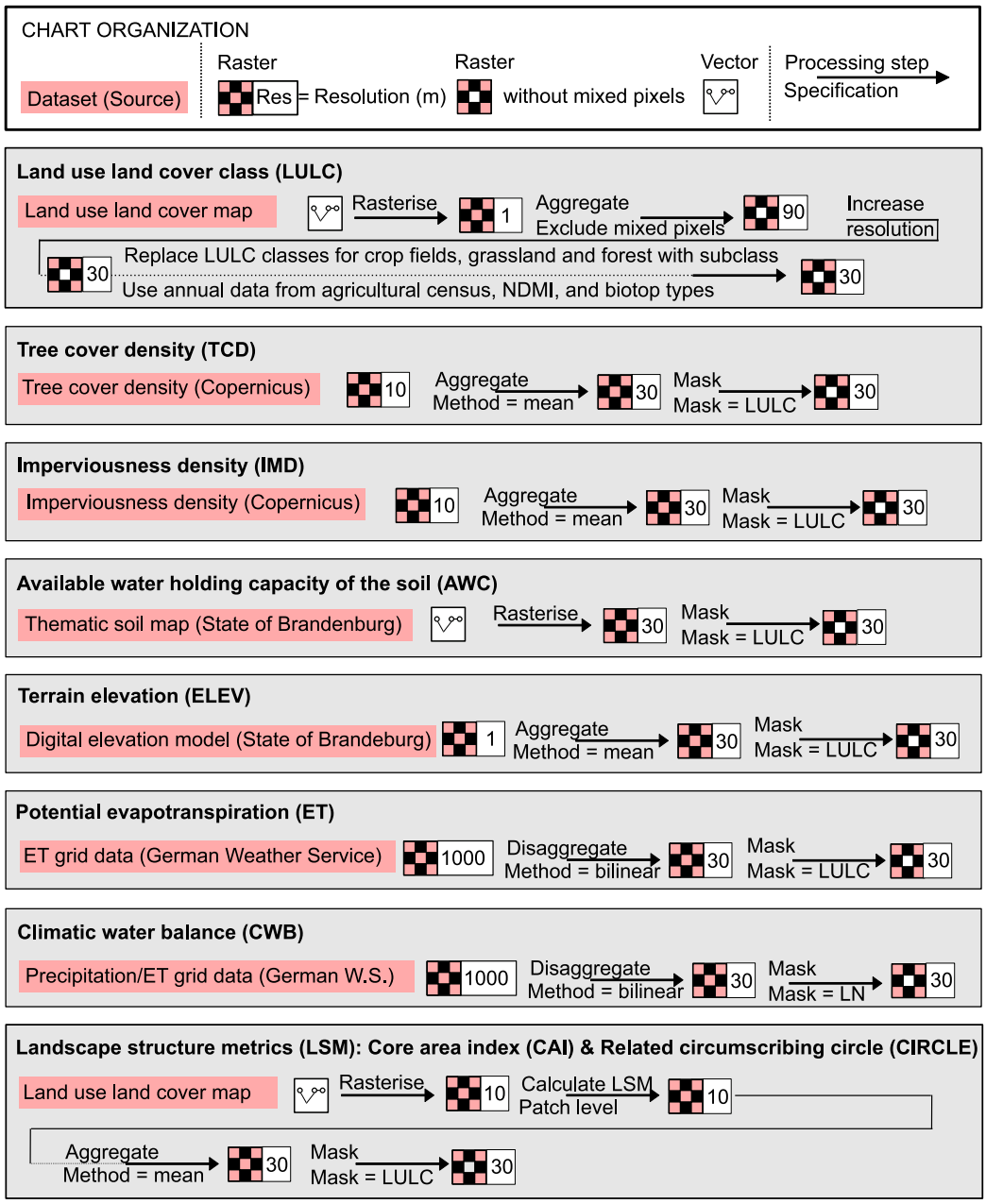

Fig. 2. Processing of the predictor variables.

the expected difference between the levels i and $i-1$ in the form of a proportion of the overall difference b (Bürkner and Charpentier, 2020). The advantage of this approach over coding AWC as a nominal predictor is that the unknown differences between the nine levels of AWC are estimated by the model.

The priors for the group-level effects, the family-specific parameters σ and ν and for the simplex were taken from the default in the library brms. That is a student_t prior (3, 0, 2.5) for the standard deviation of the group-level effects, a gamma(2, 0.1) prior for ν and a dirichlet(1) prior for the simplex. For the population-level effects, we used weakly informative normal (0,1) priors because it is very unlikely that these effects lie outside the 0 ± 2 range.

2.3.5. Model prediction for evaluation of measures

We used the fitted model to predict the cooling effect of the measures during the vegetation period. For this purpose, the predictors were assigned values that characterise the state of an area before and after (hypothetical) implementation of the measures. We based this on reasonable assumptions or observed conditions from our study area (Appendix E).

The effectiveness of the measures is subject to both temporal and spatial variation. The first is due to differences in meteorological conditions and seasonal effects. Spatial variation arises partly because predictor values vary spatially among the nearly 60,000 plots (Section 2.2). Second, not all measures affect the entire area of a plot (Fig. 3).

To deal with temporal variation, we can predict LST for each of the 39 scenes and observe the spread of the predictions. Thus, because $SCENE$ was a predictor in our model, scene-specific influences of environmental conditions not captured in our population-level predictors can also be mapped to LST. These include, for example, seasonal differences in the degree of cover of arable land or in the foliage of

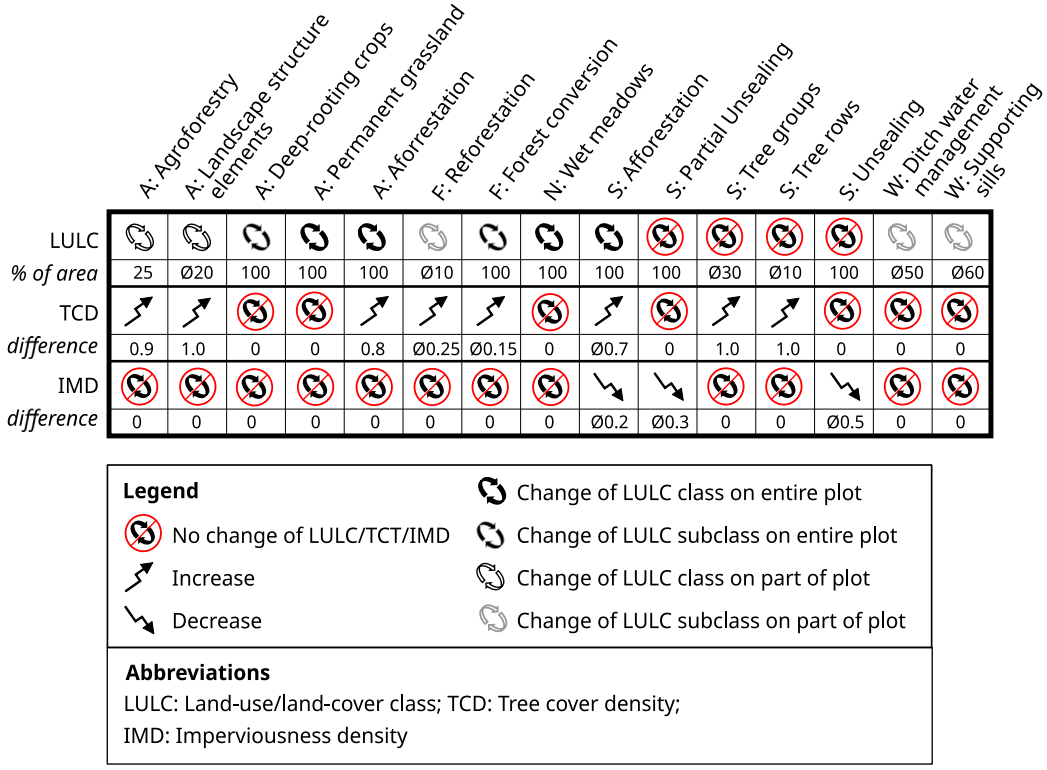

Fig. 3. Change in predictor values before and after hypothetical measure implementation. The landscape structure metrics CAI and $CIRCLE$ were also specified on the basis of their current values and the values that can be expected after implementation. Measure "organic fertilisation" does not fit into the scheme; its parametrisation is described in Appendix E.

deciduous trees. The predictors ET and CWB were set to scene-specific values. Their spatial differences were not considered, i.e., we passed spatial averages into the predictions. All other predictors were assigned to fixed (static or mean) values (Fig. 3). Since we predict each scene in the temporal approach, backscaling to actual LST values is possible. Accordingly, the differences in LST before and after hypothetical measure implementation can be expressed in Kelvin.

We also assessed differences in measure effects between individual plots, i.e., spatial variation. We therefore determined the values of the spatial predictors for each plot, where the respective measure could be implemented (Appendix A), both for the status quo and the expected state after implementation of the measures. These values were then transferred to the model prediction. This time, the values of the two climatic variables were fixed at their temporal averages for each grid cell. Both group level variables were not included.

In the final step, the predicted grid cell values were transferred to the plots (spatial vectors) by calculating (area-weighted) averages. For measures not covering the entire plot, weights were set according to the conditions of the specific plot (Appendix A, spatial variation approach) or to averages for our study area (Fig. 3, temporal variation approach). For measure "agroforestry", we assumed that 25% of the cropland is planted with woody vegetation (Fig. 3).

2.3.6. Software

All calculations were performed with R (R Core Team, 2021). The GIS algorithms required to localise the measures were programmed in GRASS GIS (GRASS Development Team, 2022) with an R interface enabled by the R library rgrass7 (Bivand et al., 2018). The LST data were processed also using GRASS GIS with R. For geospatial data processing, we used the R libraries rgdal (Bivand et al., 2023) and terra (Hijmans, 2023). Landscape structure metrics were calculated with the library landscapemetrics (Hesselbarth et al., 2019). For model building and prediction, we used the library brms (Bürkner, 2021). Plotting was done with the library ggplot2 (Wickham, 2016).

3. Results

3.1. Model performance

In Bayesian modelling, convergence diagnostics is used to check the performance of the algorithm. For the chosen model (Section 2.3.4), the diagnostics indicate convergence with $\hat{R}$ values smaller than 1.01 and effective sample sizes (much) greater than 400 (Tab. D.5, D.6, D.7). Only for two variables, sd(LULC class 10) (D.5) and ET (D.6), the $\hat{R}$ was 1.01. Since this deviation from the target $\hat{R}$ value is very small, the effective sample size is large enough and the trace plots do not show any peculiarities, we do not consider this to be overly problematic.

Posterior predictive checks using the validation data also reveal good model fit: the model -generated data resemble the observed validation data (Fig. D.7). However, due to the predictive uncertainty, the scatter in the model simulations is considerable (the y_{rep} in Fig. D.7). Therefore, we performed the predictions with at least 100 draws to reduce uncertainty in the estimated means.

The goodness of model fit can further be determined by the Bayesian version of the R^2. It is defined as the variance of the predicted values divided by the variance of predicted values plus the expected variance of the errors (Gelman et al., 2019). The Bayes R^2 value of 0.74 for the selected model confirms a good fit, but a quarter of the variance remains unexplained.

Lastly, the use of the two alternative calibration subsets (Section 2.3.4) became noticeable only in the second decimal place of the estimated coefficients. Hence, the sampling approach we chose to reduce the overall dataset has resulted in consistent results.

3.2. LST as a function of the environmental conditions

The desired evaluation of adaptation measure performance is related to the influence of each predictor on the target variable LST. To

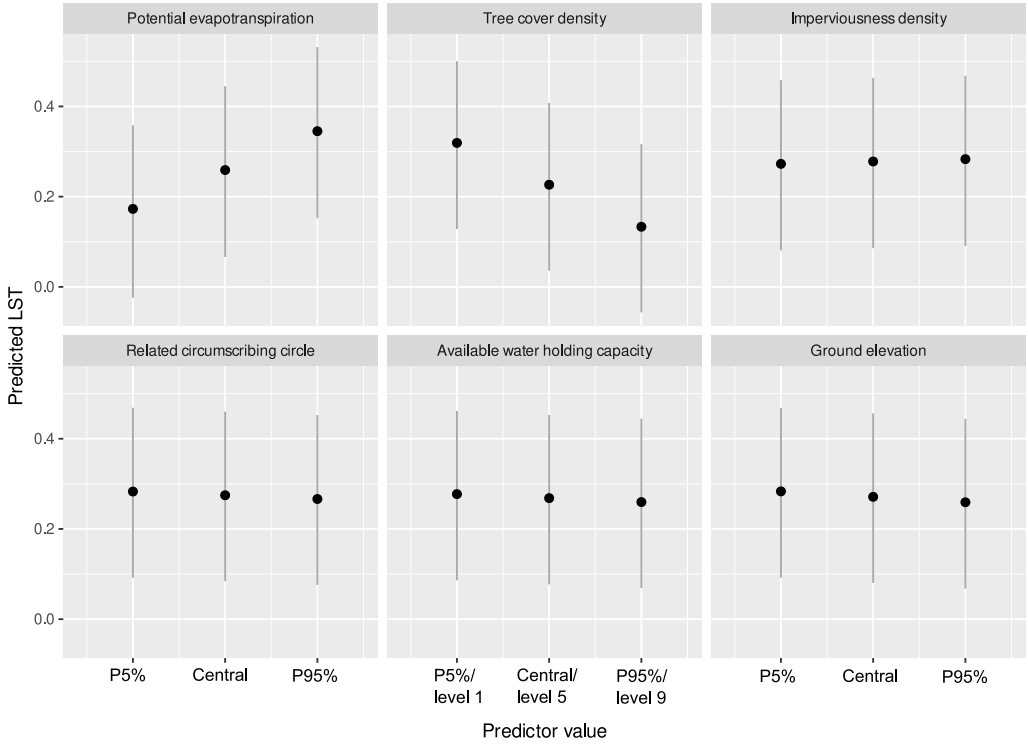

Fig. 4. Change of the predicted scaled LST where the predictors shown are varied between their 5th and 95th percentile. Central is mid-range, which we used as a measure of central tendency. All predictors except the one shown were fixed at their mean. The predicted values are drawn from the posterior distribution, taking into account scene- and ID-specific deviations in the intercepts. The bars indicate the confidence intervals of the predicted LST.

estimate variable importance, we primarily use conditional effect plots. They visualise the change in the target variable for given changes in predictor values. In interpreting the results, we consider not only the effect size but also the estimation uncertainty. This is described by the confidence intervals for the regression coefficients and the width of the posterior predictive distribution.

All population-level predictors affect LST, as indicated by confidence intervals of the estimated coefficients that do not include 0 (Tab. D.6). An important variable is the potential evapotranspiration, which is positively correlated with LST (Fig. 4). The tree cover density has a similarly large effect on LST, but the correlation is negative: with larger tree cover, LST decreases (Fig. 4). The other population-level predictors affect LST much less (Fig. 4). The direction of their effects is negative, i.e. an increase in the predictor value leads to a decrease in LST except for the imperviousness density, which increases LST as expected.

Regarding the effect of the land-use / land-cover class on LST, the ranking is as follows: Settlements and arable land appear warmer than forests and fens, while grassland areas are in between. Dry grassland was predicted to have a higher LST than fresh grassland and broad-leaved forest were the coolest class among forest types. For arable crops, winter crops as well as alfalfa were simulated slightly cooler than the summer crops. At the same time, the simulations come with wide confidence intervals. For example, the upper part of the posterior distribution of forests overlaps with the lower part of the posterior distributions of the warmer classes.

The relationship between landscape structure and LST was considered including the core area index (CAI) and the related circumscribing circle ($CIRCLE$) into the model. CAI describes area and shape of a landscape patch simultaneously: large and compact patches have larger core area. The parameter $CIRCLE$ characterises the compactness of a patch. The LST response to CAI differs among the land-use classes (Tab. D.7, Fig. 5). While in settlements and agricultural areas a larger core area coincides with an increase of the predicted LST, the opposite is true for forests and fens (Fig. 5). Particularly pronounced influences of CAI on LST are predicted for the land-use classes fens and settlements. For legumes, winter grain and dry grassland, the uncertainty of the estimation does not allow a clear assessment (Tab. D.7). The influence of $CIRCLE$ on the LST is much smaller than that of CAI (Fig. 4).

We used the climatic water balance of the month before a satellite overflight (CWB), as a simple drought indicator. We expected that the LULC class modulates the LST response to this variable (Section 2.3.2). In fact, LST in settlements and fresh grassland does not seem to respond to drought situations, while for all other LULC classes, LST increases with lower water availability (Fig. 5). It is noteworthy that especially the arable crops react very differently to this factor, with legumes and sunflowers being particularly sensitive (Fig. 5).

Considering all population-level predictors together and given the data and model at hand, a ranking of predictor importance can be established (Table 4). This ranking is confirmed by valid earlier model candidates. For example, ET and TCD were important in all of them.

The model also includes the group-level predictors $SCENE$ and ID. They account for the fact that some of the variance can be attributed to the temporal and spatial groups in our data. The importance of these predictors is given by the intra-class correlation (ICC). It can be interpreted as the proportion of explained variance that is due to the group-level effects. Hence, if the ICC is close to 0, the grouping contains no information. If, on the other hand, it tends towards 1, all observations in a group are identical (Gelman and Hill, 2006). In our model, the ICC is 0.22 with a 95% confidence interval of [0.1 0.31] – the grouping definitely contains information. When we calculate the ICC separately for each group-level predictor, their contribution is similar: an ICC of 0.13 (CI 95% [0.03 0.21]) for ID and 0.11 (CI 95% [-0.02 0.22]) for $SCENE$. Note that the ICC is more uncertain for $SCENE$ than for ID as indicated by the confidence interval for the ICC containing 0. The importance of the two predictors is further supported by the confidence intervals for their standard deviation estimates (Tab. D.5).

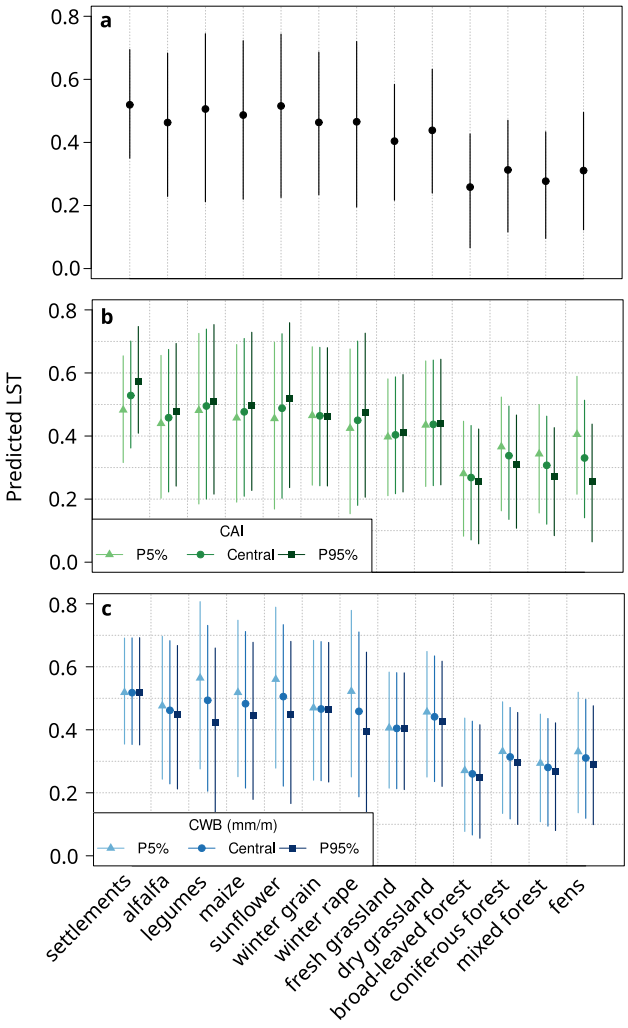

Fig. 5. Conditional effects plots for *LU LC* (a), the interaction between LULC and CAI (b), and the interaction between LULC and CWB (c). Plot (a) shows the predicted scaled LST for each LULC class, while plots (b) and (c) illustrate the change of the predicted scaled LST where CAI and CWB, respectively, are varied between their 5th percentile, central, and 95th percentile. All other predictors were fixed to LULC-specific means. The predicted values are drawn from the posterior distribution, taking into account scene- and ID-specific deviations in the intercepts. The bars indicate the confidence intervals of the predicted LST.

Table 4
Classification of predictor importance based on the magnitude of the LST change (Figs. 4, 5) and on the credible intervals of the parameter estimates (Appendix D).

Predictor	Land-use/land-cover class	Importance		
		H[a]	M[b]	L[c]
Potential evapotranspiration		×		
Climatic water balance	Settlements			×
	Arable land: alfalfa			×
	Arable land: legumes	×		
	Arable land: maize		×	
	Arable land: sunflower	×		
	Arable land: winter cereals			×
	Arable land: winter rape	×		
	Grassland: fresh			×
	Grassland: dry			×
	Forest: broad-leaved			×
	Forest: coniferous		×	
	Forest: mixed			×
	Fens			×
Land-use/land-cover class		×		
Tree cover density		×		
Imperviousness density			×	
Core area index	Settlements	×		
	Arable land: alfalfa		×	
	Arable land: legumes			×
	Arable land: maize		×	
	Arable land: sunflower		×	
	Arable land: winter cereals			×
	Arable land: winter rape		×	
	Grassland: fresh		×	
	Grassland: dry			×
	Forest: broad-leaved		×	
	Forest: coniferous		×	
	Forest: mixed		×	
	Fens	×		
Related circumscribing circle			×	
Aval. water holding capacity			×	
Terrain elevation			×	

[a] H: High - scaled LST difference ≥0.1 and confidence intervals do not include 0.
[b] M: Medium - scaled LST difference [>0, <0.1] and confidence intervals do not include 0.
[c] L: Low - scaled LST difference → 0 and confidence intervals include 0.

3.3. Assessment of adaptation measures' performance

3.3.1. Temporal variation of cooling effects

We first consider the measure effect, taking into account its temporal variation. We therefore predicted the status quo and the new state after hypothetical measure implementation for each scene with its specific climatic conditions. All other predictors were set to spatial averages. The resulting ranking of measures is based on their average effect in time, ignoring spatial variation among plots (Fig. 6).

The three most effective measures, with average cooling capacities of 3 to 3.5 K, require a change in land use — from cropland or urban wasteland to forest or from grassland to fens (Fig. 3; note that the measure "wet meadows" is parametrised as fens). The remaining measures achieve an average cooling effect of up to 2 K (Fig. 6). They are associated with a reduction in surface sealing, an increase in soil water holding capacity, the installation of tree rows or groups and a change from dry to fresh grassland (Fig. 6).

Measure "reforestation of degraded forest patches" ranks in the lower end, which is most likely due to the low average portion of degraded forest patches within a forest stand (Fig. 3). The effect of organic fertilisation also appears to be quite limited, since the associated increase in water holding capacity is limited (Appendix E). In addition, the influence of the predictor AWC on the LST is also rather moderate (Fig. 4). The measure "cultivation of deep-rooting arable crops" shows no effect at all, which can be explained by our choice of crops in the simulated crop rotations: both the conventional and the measure-specific crop rotations contain crops with higher LST (legumes in the conventional and sunflowers in the specific rotation, see Fig. 5).

3.3.2. Comparison with spatial variation of cooling effects

We also assessed differences in measure effects between individual plots, i.e., spatial variation. This time, we set the climatic parameters to their spatially varying temporal averages. The other predictors were given their plot-specific values before and after implementation of the measures (Section 2.3.5).

The performance ranking for the three most efficient measures remains unchanged for the spatial approach compared to the temporal approach (Fig. 6). Some slight differences in ranking characterise the remaining measures. Particularly noteworthy are the numerous outliers in the direction of both higher and lower effectiveness, especially for the measures "afforestation of urban brownfields", "tree rows in settlements", "forest conversion", "landscape structure elements" and

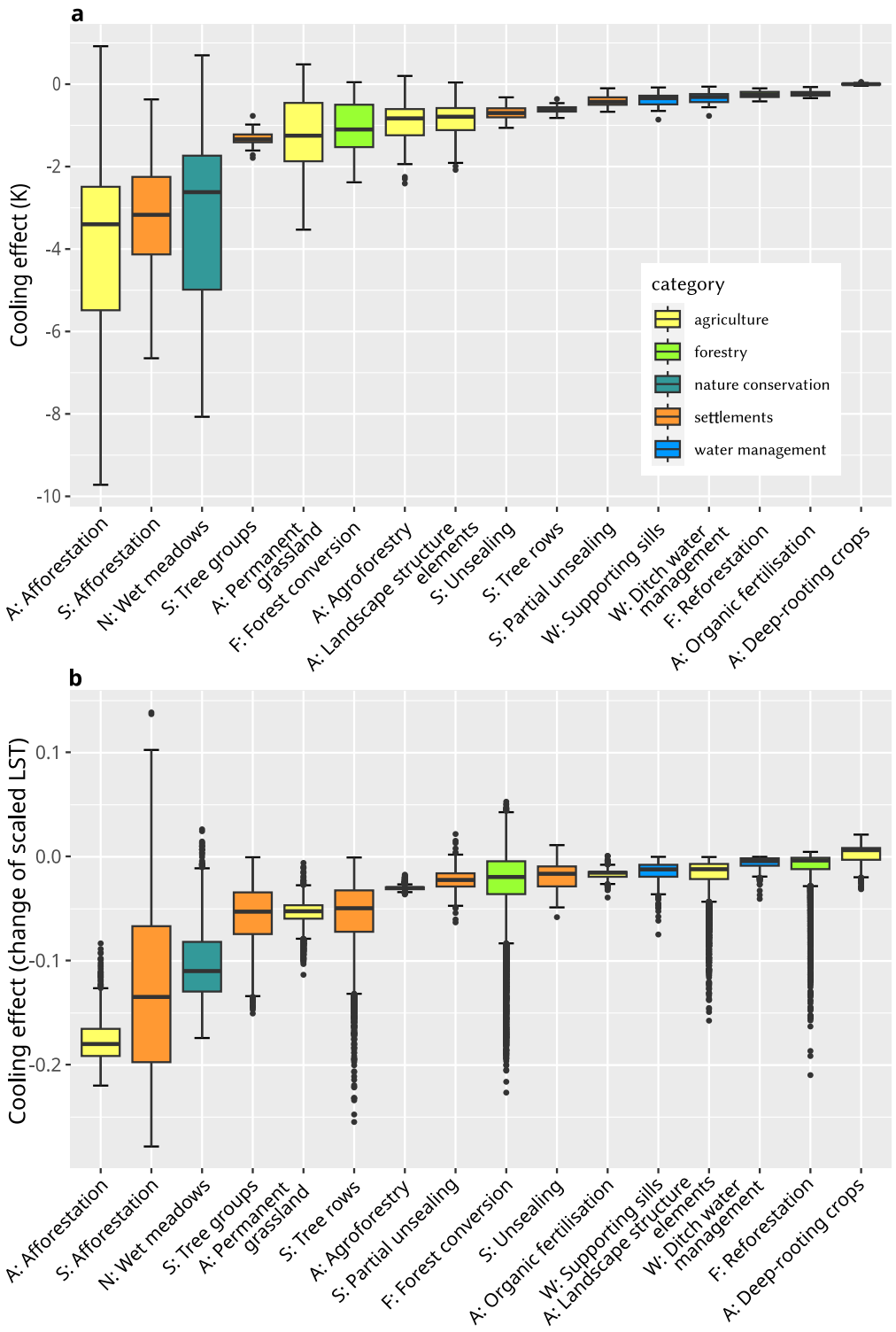

Fig. 6. Predicted cooling effects of the adaptation measures, temporal variation (a) and spatial variation (b).

"reforestation of degraded forest patches". This wide variation in the impact of these measures is the result of the different sources of spatial variation (Tab. F.9). For instance, the range of area share of the measure landscape structure elements is extremely wide, between slightly above 0 and nearly 100% of a plot that could accommodate this measure.

The spatial approach to measure evaluation accounts for plot-specific differences in predictor values for mean climatic conditions. It is therefore most suitable for deciding where which measure should be implemented most appropriately. The time-varying prediction can then be used to incorporate possible seasonal and climatic effects into the evaluation.

When comparing the contributions of both sources of variation, the following picture emerges: for most measures, the contribution of spatial variation is larger than that of temporal variation (Tab. F.9). However, in the case of measures related to agriculture, the opposite is

true, which is already indicated by the large importance of the group-level effect $SCENE$(D.5) on the LST footprint of many crops. Seasonal differences in crop growth and cover could explain this observation.

4. Discussion

4.1. Drivers of land surface temperature

Our analysis revealed settlements as the warmest LULC class, warmer than forests or cropland. This is a widely supported finding, with corresponding examples from all around the world (e.g. Alavipanah et al., 2015; Das et al., 2020; Seeberg et al., 2022; Wickham et al., 2012). Here, the domination of surfaces from which only ponding water can evaporate leads to a significant turnover of radiation into sensible heat, with increasing temperature as a consequence. Using light colours on building walls and roofs is an ancient technique to increase the albedo and thus reduce the turn-over towards higher reflectance in regions that suffer from high temperatures during summer.

In vegetated areas, evapotranspiration governs the energy conversion at the land surface (Sheil, 2018). It is therefore not surprising that our analysis identified ET as a dominating factor influencing LST. There is also a close relationship between solar radiation and LST (Bertoldi et al., 2010), with solar radiation being one of the key factors for potential evapotranspiration (Priestley and Taylor, 1972).

The ability of a land surface to evaporate or transpire water is a primary characteristic that governs LST. It explains why forests are cooler than crop- or grassland during daytime (Ba et al., 2024) and that the most widely recommended strategy for mitigating increasing LST in urban areas is to increase vegetation and green areas (Patel et al., 2024). For the same reason, sealing or unsealing of land has a significant influence on LST (e.g. Song et al., 2014; Seeberg et al., 2022). In our analysis, this reflects in the positive correlation between imperviousness density and LST. Similarly, research has shown that densely clustered vegetation patterns are more effective at reducing LST than scattered ones (Fan et al., 2015; Kim et al., 2016).

Using the group-level variables $SCENE$ and ID, we included additional error terms in the model. They account for the hierarchical nature of the data: each pixel belongs to a particular unit in space (e.g., all pixels in a field or forest stand) and to one of the 39 satellite scenes. Their proven significance suggests that the sometimes substantial differences in LST between LULC classes do not occur everywhere (predictor ID) or at all times (predictor $SCENE$). Using them in the model also helps to compensate for the fact that not all factors affecting LST could be included in the model. For example, the predictor "tree cover density" is actually variable over time, but was implemented as a static variable (Table 2). Since $SCENE$ was used to estimate a scene-specific intercept for each LULC class, this temporal variance can thus be accounted for to some extent. In general, the inclusion of the group-level predictors resulted in a more realistic representation of uncertainty in the model estimates of population-level effects. For instance, if we had calculated the confidence intervals in the conditional effects plots without taking group-level effects into account, the overlap among the LULC classes (Fig. 5) would not have emerged.

4.2. Adaptation measure efficiency

In many studies devoted to understanding LST, the focus is on mitigation of urban heat islands (e.g. Alavipanah et al., 2015; Mehmood et al., 2023; Seeberg et al., 2022; Selim et al., 2023). In our study, we transferred these approaches to rural areas to predict adaptation measure effectiveness. Seeberg et al. (2022)'s approach to evaluating the success of heat stress interventions and Selim et al. (2023)'s work on the cooling potential of green spaces took a similar approach in the urban context, albeit retro- rather than prospective.

During a hot summer day, the temperature regime of a forest is known to be cooler than that of an open agricultural landscape (Müttrich, 1897; Procházka et al., 2019; Ghafarian et al., 2022). Due to the large influence of tree cover density and LULC class on LST, those measures that significantly increase tree cover or result in a change in LULC class are ranked highest. Consequently, the effectiveness of measures "agroforestry" and "landscape structure elements" increases with a greater density of these elements. For example, if the agroforestry strips were placed every 24 m, this would result in an increase of the cooling effect to 1.1 K on average. Ghafarian et al. (2024) analysed small woody features in an agricultural landscape close to our study site and concluded that a significant LST decrease was identified when trees or woody vegetation patches had a distance smaller than 75 m. Conversely, reducing tree cover densities – in our parametrisation, tree cover was set to the maximum possible values (Fig. 3) – would significantly reduce the cooling effect. This suggests that a closed canopy and a high density of the woody vegetation elements are particularly important for these measures to be effective.

In contrast, measures have a lower effectiveness if the importance of the predictors was only moderate, such as IMD and AWC (Table 4). Among those are measures "organic fertilisation" and "unsealing" with subsequent establishment of a grass cover (Fig. 6). Moreover, if the only change in predictor values is among subclasses of $LULC$ on parts of the plots (measures "ditch water management" and "supporting sills", Fig. 3), the cooling effect appears limited (Fig. 6). A somewhat different picture could emerge if these water management measures were located on arable land and could contribute to better water supply for crops, e.g. by controlled drainage systems that allow water retention when dry periods are expected, and drainage when high soil moisture levels hamper field traffic or crop growth. However, this assessment was not possible in this study: NDMI, which we used as a groundwater influence proxy, depends not only on water supply, but also on crop type. Our database was too limited to further investigate these aspects.

The predicted cooling effects per measure (Fig. 6) cover a wide range, which furthermore depends on the season. For example, the cooling effect of measures that increase the proportion of trees is lower in May and / or in September than in the summer months (Fig. G.8). Reasons for this observation are the seasonality of the drivers for evapotranspiration and of the presence of leaves – the primary transpiring organs – on the deciduous trees and shrubs. Distinct seasonal patterns of LST differences between forest and crop- / grassland were also reported in Ba et al. (2024). Likewise, dense vegetation was shown to turn into a warmer environment in winter, due to heat storage in the tree mass, limited long-wave radiation, and ceased transpiration (Zellweger et al., 2019). The effect of improved water retention with the measures "ditch water management" and "supporting sills" seems to generally decrease towards September, which is again related to the decrease in evapotranspiration, but most likely also to the decrease in ditch- and groundwater levels as the summer progresses. Due to the limited number of available thermal scenes, these seasonal results should be interpreted with caution. However, they support that the cooling effect of a measure varies over time and that this time component varies for individual measures.

In addition to the seasonal differences, the influence of the vegetation cover on the LST is subject to day-night conversions (Peng et al., 2014). It is well known that the cooling effect of forests during the day can turn into a warming effect during the night, which can even lead to a net warming effect of forests, depending on the forest type and geographical location (Ba et al., 2024). Our measures aim to dampen the LST peaks during the day and thus reduce water loss from the landscape. However, due to the diurnal shifts, no general reduction in LST to mitigate regional climate change can be attributed to them without further evaluation.

The plot-specific assessment can indicate where which measures should be prioritised in terms of benefits. If the aim is to achieve an even distribution of cooling effects over the course of the year, or if a cooling effect is particularly relevant in the summer months, for example, the seasonal differences in the measure performance would also be of interest for practical implementation.

Of course, other criteria need to be taken into account in addition to effectiveness, such as costs, synergies with nature conservation, or local constraints. In a cost–benefit analysis of water retention measures, which also covered eastern Germany, it was determined that measures in croplands pay off the most (Sušnik et al., 2022). This study focus es on the benefit side, while the inclusion of costs represents the next step (Hecker et al., 2024).

4.3. Reliability of statistical LST-based measure evaluation

The use of satellite data of LST has limitations. The Landsat 8 Collection 2 Level 2 thermal data are transferred into LST using emissivity data by the ASTER Global Emissivity dataset (ASTER GED). The ASTER GED provides emissivity data from 2000–2008, derived from factors like vegetation cover. If land cover changed before 2013 when LST data became available, incorrect emissivities might be used, leading to erroneous LST data. Detecting changes in NDVI could address this, but was beyond the scope of our analysis. Another limitation of the satellite data is their fixed return interval, which is at 10 AM in our study area. This overflight time does not correspond to the time of day when evaporation normally reaches its maximum. Therefore, the reported LST differences in response to the measures are strictly valid only for this time window.

The success and reliability of the statistical modelling heavily depend on the decisions made throughout the process from data acquisition, model development, to model prediction. Among those are the choice of the population- and group-level predictors, interaction terms, response families, priors etc. It is particularly important to emphasise that a whole range of options is already available when selecting the model tool. For example, a machine learning (ML) approach could have been chosen as an alternative way for predicting adaptation measure performance. We decided against ML because we put emphasis in model interpretability and uncertainty understanding (Gross et al., 2020). However, it is quite possible that the predictive performance can be improved by choosing ML, because e.g. it omits the specification of interaction terms. It would certainly be interesting to compare alternative approaches in a separate study.

Another point regarding the reliability of the results addresses the parametrisation of model predictions. Due to the inevitable simplification of reality, parametrisation comes with numerous assumptions and limitations. For instance, the LST for the status quo of arable land might be overestimated in the presence of linearly shaped woody vegetation which is not included in our land cover data (Appendix A). Furthermore, we assigned a core area index of 0 for measures "agroforestry" and "landscape structure elements", which represents an extrapolation since the model dataset does not contain such low CAI values (Table 2). The resulting potential error is 0.4 K at maximum, as indicated by predictions for these measures using the lowest CAI in the model dataset. Given these and other uncertainties, we have avoided making sharp distinctions in interpreting the measures' ranking.

To conclude, the presented model is the best model we could create. However, it certainly will be worth an update once more / better / other data will become available. This relates both to the satellite scenes as well as to the geospatial data that serve for predictor derivation. The limited importance of the water-holding capacity of the soil on LST might also be related to the coarse map resolution and classification of originally numerical values in the thematic soil map, which was used to derive AWC (Fig. 2). Still missing information such as seasonality of tree cover density and more finely resolved data on soil water retention could be incorporated in future model candidates.

5. Conclusion

Our results indicate that the process of evapotranspiration by vegetation and enhanced water retention make a significant contribution to local cooling of the land surface. Moreover, the quality of the model output was shown to be suitable for the desired ex-ante assessment of the impact of climate adaptation measures. We summarise our results by answering the research questions posed in the introduction:

1. With the included predictors and the fitted model, a large part of the variance in land surface temperature could be explained. The most important predictors were the potential evapotranspiration, the tree cover density, and the land-use / land-cover (LULC) class. Both landscape structure and drought severity (predictor CWB) influence LST, but only for some LULC classes. The other predictors are of moderate to minor importance in our rural study region.
2. By implementing nature-based climate adaptation measures, evapotranspiration and water retention can be influenced if the measures are designed in such a way that they strengthen these processes. This includes, firstly, the introduction of plants into land use systems that have a high evapotranspiration capacity. These include woody plants in particular. Since evapotranspiration is an area-based process, the amount of area that can be provided with woody plants is crucial for the cooling effect. Adequate water supply is also critical to evapotranspiration. If water retention in the landscape can be improved, for example by wetland restoration, largely unrestricted evaporation is ensured even in summer, which also results in high cooling performance. Some of the measures we have considered show only a minor effect. This is mainly due to only a gradual change of a plot's condition (e.g. change of a LULC subclass compared to a LULC class), a low area coverage of the measure, or the subordinate importance of the predictors that can be influenced by the measure.
3. The parallel evaluation of different measures is a valuable tool for decision support on climate adaptation. The results can be applied to the different land use sectors to identify the most promising measures for a given area. In addition, they can be used in spatial planning and in the management of subsidy allocations. By including multiple satellite scenes in the analysis, it is also possible to take into account the temporal dynamics of the cooling effects within the course of the year. We are confident that a comparable modelling approach can also be used to assess potential climate adaptation measures in other regions. The reliability of the results will depend on the quality and availability of the data, while the general relationships should also apply elsewhere.

CRediT authorship contribution statement

Beate Zimmermann: Writing – review & editing, Writing – original draft, Visualization, Methodology, Funding acquisition, Formal analysis, Conceptualization. **Sarah Kruber:** Writing – review & editing, Writing – original draft, Methodology, Formal analysis. **Claas Nendel:** Writing – review & editing. **Henry Munack:** Writing – review & editing, Visualization, Methodology, Funding acquisition, Conceptualization. **Christian Hildmann:** Writing – review & editing, Visualization, Supervision, Funding acquisition, Conceptualization.

Declaration of competing interest

The authors declare that they have no known competing financial interests or personal relationships that could have appeared to influence the work reported in this paper.

Data availability

Satellite images of Landsat 8 the Copernicus data are available for free use (https://earthexplorer.usgs.gov/, https://land.copernicus.eu/en). Weather data from the German Weather Service are available via https://www.dwd.de/EN/ and also without use restriction. Data for the local allocation of measures is made freely available by the Federal State of Brandenburg. In addition, freely available data of the tracks from Deutsche Bahn and roads and paths from OpenStreetMap have been used. Data with use restriction are the land cover model of Germany, locations of ditches and farm dams, the mean groundwater level map, building outlines and forest site characteristics map of the federal state of Brandenburg.

Acknowledgements

We would like to thank our project partners from the Elbe-Elster county for their cooperation and the provision of data through their GIS system. We also thank Dr. Dirk Knoche, Research Institute for Post-Mining Landscapes, for his support in parametrising the forestry measures.

Funding

This work was supported by the German Federal Ministry of Education and Research (BMBF, Grant number 01LR2004B).

Appendix. Supplementary data

Supplementary material related to this article can be found online at https://doi.org/10.1016/j.jenvman.2024.121595.

References

Alavipanah, S., Wegmann, M., Qureshi, S., Weng, Q., Koellner, T., 2015. The role of vegetation in mitigating urban land surface temperatures: A case study of Munich, Germany during the warm season. Sustainability 7, 4689–4706. http://dx.doi.org/10.3390/su7044689.

Amt für Statistik Berlin-Brandenburg, 2022. Statistischer bericht, flächenerhebung nach art der tatsächlichen nutzung im land brandenburg 2021. URL https://download.statistik-berlin-br{and}enburg.de/4bb421915ed644bc/1b39ca17cfc6/SB_A05-03-00_2021j01_BB.pdf. (assessed 24 2023).

Amt für Statistik Berlin-Brandenburg, 2023. Statistischer bericht, bevölkerungsentwicklung und bevölkerungsstand im land brandenburg dezember 2022. URL https://download.statistik-berlin-br{and}enburg.de/8ee0bad9b1168256/a3df42d855eb/SB_A01-07-00_2022m12_BB.pdf. (assessed 24 2023).

Ba, S., Wang, W.J., Sun, H., Bao, S.G., Zhang, H., He, H.S., 2024. The cooling and warming effects of potential forest transition on local land surface temperature in northeast china. Ecol. Indic. 159, 111645. http://dx.doi.org/10.1016/j.ecolind.2024.111645.

Baessler, C., Klotz, S., 2006. Effects of changes in agricultural land-use on landscape structure and arable weed vegetation over the last 50 years. Agric. Ecosyst. Environ. 115, 43–50. http://dx.doi.org/10.1016/j.agee.2005.12.007.

Bednar-Friedl, B., Biesbroek, R., Schmidt, D.N., Alexander, P., Børsheim, K.Y., Carnicer, J., Georgopoulou, E., Haasnoot, M., Le Cozannet, G., Lionello, P., Lipka, O., Möllmann, C., Muccione, V., Mustonen, T., Piepenburg, D., Whitmarsh, L., 2023. Europe. In: Climate Change 2022 – Impacts, Adaptation and Vulnerability. Contribution of Working Group II To the Sixth Assessment Report of the Intergovernmental Panel on Climate Change. Cambridge University Press, pp. 1817–1928. http://dx.doi.org/10.1017/9781009325844.015.

Bertoldi, G., Notarnicola, C., Leitinger, G., Endrizzi, S., Zebisch, M., Chiesa, S.D., Tappeiner, U., 2010. Topographical and ecohydrological controls on land surface temperature in an alpine catchment. Ecohydrology 3, 189–204. http://dx.doi.org/10.1002/eco.129.

Bivand, R., Keitt, T., Rowlingson, B., 2023. Rgdal: Bindings for the 'Geospatial' data abstraction library. http://rgdal.r-forge.r-project.org, https://gdal.org, https://proj.org, https://r-forge.r-project.org/projects/rgdal/.

Bivand, R., Krug, R., Neteler, M., Jeworutzki, S., 2018. rgrass7: Interface between GRASS 7 geographical information system and R. URL: https://CRAN.R-project.org/package=rgrass7. r package version 0.1-12.

Bürkner, P.C., 2021. Bayesian item response modeling in R with brms and Stan. J. Stat. Softw. 100, 1–54. http://dx.doi.org/10.18637/jss.v100.i05.

Bürkner, P.C., Charpentier, E., 2020. Modelling monotonic effects of ordinal predictors in Bayesian regression models. Br. J. Math. Stat. Psychol. 73, 420–451. http://dx.doi.org/10.1111/bmsp.12195.

Copernicus, 2022. Copernicus: Globally, the seven hottest years on record were the last seven; carbon dioxide and methane concentrations continue to rise. URL https://climate.copernicus.eu/copernicus-globally-seven-hottest-years-record-were-last-seven. (assessed 18 2023).

Das, D.N., Chakraborti, S., Saha, G., Banerjee, A., Singh, D., 2020. Analysing the dynamic relationship of land surface temperature and landuse pattern: A city level analysis of two climatic regions in India. City Environ. Interact. 8, 100046. http://dx.doi.org/10.1016/j.cacint.2020.100046.

Du, S., Xiong, Z., Wang, Y.C., Guo, L., 2016. Quantifying the multilevel effects of landscape composition and configuration on land surface temperature. Remote Sens. Environ. 178, 84–92. http://dx.doi.org/10.1016/j.rse.2016.02.063.

Fan, C., Myint, S., Zheng, B., 2015. Measuring the spatial arrangement of urban vegetation and its impacts on seasonal surface temperature. Prog. Phys. Geogr.: Earth Environ. 39, 199–219. http://dx.doi.org/10.1177/0309133314567583.

Gelman, A., Goodrich, B., Gabry, J., Vehtari, A., 2019. R-squared for bayesian regression models. Am. Stat. 73, 307–309. http://dx.doi.org/10.1080/00031305.2018.1549100.

Gelman, A., Hill, J., 2006. Data Analysis using Regression and Multilevel/Hierarchical Models. In: Analytical Methods for Social Research, Cambridge University Press, http://dx.doi.org/10.1017/CBO9780511790942.

Gelman, A., Vehtari, A., Simpson, D., Margossian, C.C., Carpenter, B., Yao, Y., Kennedy, L., Gabry, J., Bürkner, P.C., Modrák, M., 2020. Bayesian workflow. http://dx.doi.org/10.48550/arXiv.2011.01808, preprint at 10.48550/arXiv.2011.01808.

Ghafarian, F., Ghazaryan, G., Wieland, R., Nendel, C., 2024. The impact of small woody features on the mesoclimate in an agricultural landscape. Agricult. Forest Meteorol. 349, 109949. http://dx.doi.org/10.1016/j.agrformet.2024.109949.

Ghafarian, F., Wieland, R., Lüttschwager, D., Nendel, C., 2022. Application of extreme gradient boosting and Shapley additive explanations to predict temperature regimes inside forests from standard open-field meteorological data. Environ. Model. Softw. 156, 105466. http://dx.doi.org/10.1016/j.envsoft.2022.105466.

GRASS Development Team, 2022. Geographic Resources Analysis Support System (GRASS GIS) Software, Version 8.2. Open Source Geospatial Foundation, URL https://grass.osgeo.org.

Gross, D.P., Steenstra, I.A., Harrell, F.E., Bellinger, C., Zaïane, O., 2020. Machine learning for work disability prevention: Introduction to the special series. J. Occup. Rehabil. 30, 303–307. http://dx.doi.org/10.1007/s10926-020-09910-1.

Hecker, L.P., Wätzold, F., Sturm, A., Zimmermann, B., Kruber, S., Hildmann, C., 2024. Keep cool in a changing climate: An integrated modelling procedure to identify cost-effective, spatially differentiated land-use and land-cover measures to mitigate rising temperature in rural landscapes. http://dx.doi.org/10.21203/rs.3.rs-3904821/v1.

Hesselbarth, M.H.K., Sciaini, M., With, K.A., Wiegand, K., Nowosad, J., 2019. Landscapemetrics: an open-source R tool to calculate landscape metrics. Ecography 42, 1648–1657. http://dx.doi.org/10.1111/ecog.04617.

Hesselmann, G., 2018. Applying linear mixed effects models (LMMs) in within-participant designs with subjective trial-based assessments of awareness—a caveat. Front. Psychol. 9, http://dx.doi.org/10.3389/fpsyg.2018.00788.

Hesslerová, P., Huryna, H., Pokorný, J., Procházka, J., 2018. The effect of forest disturbance on landscape temperature. Ecol. Eng. 120, 345–354. http://dx.doi.org/10.1016/j.ecoleng.2018.06.011.

Hesslerová, P., Pokorný, J., Brom, J., 2013. Daily dynamics of radiation surface temperature of different land cover types in a temperate cultural landscape: Consequences for the local climate. Ecol. Eng. 54, 145–154. http://dx.doi.org/10.1016/j.ecoleng.2013.01.036.

Hijmans, R.J., 2023. Terra: Spatial data analysis.

Hildmann, C., Zimmermann, B., Schlepphorst, R., Rösel, L., Kleinschmidt, F., Kruber, S., Lukas, S., Joshi, D.C., Hecker, L.P., Witt, J.C., Sturm, A., Wätzold, F., 2022. Measures for adaptation to climate change through water retention and cooling by transpiration: A catalogue of measures for a drought-prone area in eastern Germany. http://dx.doi.org/10.5281/zenodo.6811079, preprint at DOI: 10.5281/zenodo.6811079.

Ionita, M., Nagavciuc, V., Kumar, R., Rakovec, O., 2020. On the curious case of the recent decade, mid-spring precipitation deficit in central Europe. NPJ Clim. Atmos. Sci. 3, 49. http://dx.doi.org/10.1038/s41612-020-00153-8.

Kim, J.H., Gu, D., Sohn, W., Kil, S.H., Kim, H., Lee, D.K., 2016. Neighborhood landscape spatial patterns and land surface temperature: An empirical study on single-family residential areas in Austin, Texas. Int. J. Environ. Res. Public Health 13 (880), http://dx.doi.org/10.3390/ijerph13090880.

Landesamt für Umwelt Brandenburg, 2009. Flächendeckende Biotop- und landnutzungskartierung (btln) im land brandenburg - CIR-Biotoptypen 2009. URL https://lfu.br{and}enburg.de/lfu/de/aufgaben/natur/biotopschutz/biotopkartierung/biotop-und-l{and}nutzungskartierung/. (assessed 21 2023).

Makarieva, A.M., Nefiodov, A.V., Nobre, A.D., Baudena, M., Bardi, U., Sheil, D., Saleska, S.R., Molina, R.D., Rammig, A., 2023. The role of ecosystem transpiration in creating alternate moisture regimes by influencing atmospheric moisture convergence. Glob. Change Biol. 29, 2536–2556. http://dx.doi.org/10.1111/gcb.16644.

Makarieva, A.M., Nefiodov, A.V., Nobre, A.D., Sheil, D., Nobre, P., Pokorný, P., Li, B.L., 2022. Vegetation impact on atmospheric moisture transport under increasing land-ocean temperature contrasts. Heliyon 8, e11173. http://dx.doi.org/10.1016/j.heliyon.2022.e11173.

McElreath, R., 2020. Statistical Rethinking. Chapman and Hall/CRC, http://dx.doi.org/10.1201/9780429029608.

Mehmood, M.S., Rehman, A., Sajjad, M., Song, J., Zafar, Z., Shiyan, Z., Yaochen, Q., 2023. Evaluating land use/cover change associations with urban surface temperature via machine learning and spatial modeling: Past trends and future simulations in dera ghazi khan, pakistan. Front. Ecol. Evol. 11, http://dx.doi.org/10.3389/fevo.2023.1115074.

Müttrich, A., 1897. Beobachtungen. Springer, Berlin.

Patel, S., Indraganti, M., Jawarneh, R.N., 2024. A comprehensive systematic review: Impact of land use/ land cover (lulc) on land surface temperatures (lst) and outdoor thermal comfort. Build. Environ. 249, 111130. http://dx.doi.org/10.1016/j.buildenv.2023.111130.

Peng, S.S., Piao, S., Zeng, Z., Ciais, P., Zhou, L., Li, L.Z., Myneni, R.B., Yin, Y., Zeng, H., 2014. Afforestation in China cools local land surface temperature. Proc. Natl. Acad. Sci. USA 111, 2915–2919. http://dx.doi.org/10.1073/pnas.1315126111.

Pfeifer, S., Bathiany, S., Rechid, D., 2021. Klimaausblick Elbe-ELster. Technical Report, Climate Service Center Germany (GERICS), URL https://www.gerics.de/klimaausblick-l{and}kreise.

Priestley, C.H.B., Taylor, R.J., 1972. On the assessment of surface heat flux and evaporation using large-scale parameters. Mon. Weather Rev. 100, 81–92.

Procházka, J., Pokorný, J., Vácha, A., Novotná, K., Kobesová, M., 2019. Land cover effect on water discharge, matter losses and surface temperature: Results of 20 years monitoring in the šumava mts. Ecol. Eng. 127, 220–234. http://dx.doi.org/10.1016/j.ecoleng.2018.11.030.

R Core Team, 2021. R: A Language and Environment for Statistical Computing. R Foundation for Statistical Computing, Vienna, Austria, URL https://www.R-project.org/.

Samaniego, L., Thober, S., Kumar, R., Wanders, N., Rakovec, O., Pan, M., Zink, M., Sheffield, J., Wood, E.F., Marx, A., 2018. Anthropogenic warming exacerbates European soil moisture droughts. Nat. Clim. Change 8, 421–426. http://dx.doi.org/10.1038/s41558-018-0138-5.

Seeberg, G., Hostlowsky, A., Huber, J., Kamm, J., Lincke, L., Schwingshackl, C., 2022. Evaluating the potential of landsat satellite data to monitor the effectiveness of measures to mitigate urban heat islands: A case study for Stuttgart (Germany). Urban Sci. 6, 82. http://dx.doi.org/10.3390/urbansci6040082.

Selim, S., Eyileten, B., Karakuş, N., 2023. Investigation of green space cooling potential on land surface temperature in Antalya city of Turkey. Int. Arch. Photogramm. Remote Sens. Spat. Inf. Sci. - ISPRS Arch. XLVIII-M-1-2023, 107–114. http://dx.doi.org/10.5194/isprs-archives-XLVIII-M-1-2023-107-2023.

Sheil, D., 2018. Forests, atmospheric water and an uncertain future: the new biology of the global water cycle. For. Ecosyst. 5, http://dx.doi.org/10.1186/s40663-018-0138-y.

Song, J., Du, S., Feng, X., Guo, L., 2014. The relationships between landscape compositions and land surface temperature: Quantifying their resolution sensitivity with spatial regression models. Landsc. Urban Plan. 123, 145–157. http://dx.doi.org/10.1016/j.landurbplan.2013.11.014.

Sušnik, J., Masia, S., Kravčík, M., Pokorný, J., Hesslerová, P., 2022. Costs and benefits of landscape-based water retention measures as nature-based solutions to mitigating climate impacts in eastern Germany, Czech Republic, and Slovakia. Land Degrad. Dev. 33, 3074–3087. http://dx.doi.org/10.1002/ldr.4373.

Wickham, H., 2016. Ggplot2: Elegant Graphics for Data Analysis. Springer-Verlag New York, URL https://ggplot2.tidyverse.org.

Wickham, J.D., Wade, T.G., Riitters, K.H., 2012. Comparison of cropland and forest surface temperatures across the conterminous united states. Agric. for. Meteorol. 166–167, 137–143. http://dx.doi.org/10.1016/j.agrformet.2012.07.002.

Wolff, S., Hüttel, S., Nendel, C., Lakes, T., 2021. Agricultural landscapes in Brandenburg, Germany: an analysis of characteristics and spatial patterns. Int. J. Environ. Health Res. 15, 487–507. http://dx.doi.org/10.1007/s41742-021-00328-y.

World Meteorological Organization (WMO), 2023. State of the climate in Europe 2022. URL https://library.wmo.int/idurl/4/66206. (accessed 18 September 2023).

Zellweger, F., Coomes, D., Lenoir, J., Depauw, L., Maes, S.L., Wulf, M., Kirby, K.J., Brunet, J., Kopecký, M., Máliš, F., Schmidt, W., Heinrichs, S., den Ouden, J., Jaroszewicz, B., Buyse, G., Spicher, F., Verheyen, K., De Frenne, P., 2019. Seasonal drivers of understorey temperature buffering in temperate deciduous forests across europe. Glob. Ecol. Biogeogr. 28, 1774–1786. http://dx.doi.org/10.1111/geb.12991.

Zimmermann, B., Hildmann, C., 2021. Klimawandel im landkreis elbe-elster ganz konkret: Eine analyse von daten aus der Wetterstation Doberlug-Kirchhain. URL https://www.lkee.de/media/custom/2112_8805_1.PDF?1621336033. (accessed 25 July 2023).

Zomer, R.J., Xu, J., Trabucco, A., 2022. Version 3 of the global aridity index and potential evapotranspiration database. Sci. Data 9, http://dx.doi.org/10.1038/s41597-022-01493-1.